Spin–orbit induced local band structure variations revealed by scanning tunnelling spectroscopy

2003 J. Phys.: Condens. Matter 15 S679

(http://iopscience.iop.org/0953-8984/15/5/320)

INSTITUTE OF PHYSICS PUBLISHING JOURNAL OF PHYSICS: CONDENSED MATTER

J. Phys.: Condens. Matter **15** (2003) S679–S692 PII: S0953-8984(03)54537-4

Spin–orbit induced local band structure variations revealed by scanning tunnelling spectroscopy

M Bode[1,3], A Kubetzka[1], S Heinze[1,4], O Pietzsch[1], R Wiesendanger[1], M Heide[2], X Nie[2,5], G Bihlmayer[2] and S Blügel[2]

[1] Institute of Applied Physics and Microstructure Research Center, University of Hamburg, Jungiusstrasse 11, 20355 Hamburg, Germany
[2] Institut für Festkörperforschung, Forschungszentrum Jülich, 52425 Jülich, Germany

E-mail: mbode@physnet.uni-hamburg.de

Received 9 October 2002
Published 27 January 2003
Online at stacks.iop.org/JPhysCM/15/S679

Abstract

Scanning tunnelling spectroscopy (STS) of thin Fe films on W(110) shows that the electronic structures of magnetic domains and domain walls are different. This experimental result is explained on the basis of first-principles calculations. A detailed analysis reveals that the spin–orbit induced mixing between minority d_{xy+xz} and minority d_{z^2} spin states depends on the magnetization direction and changes the local density of states in the vacuum detectable by STS. The effect scales in second or fourth order with the magnetization angle relative to the easy axis. Our finding implies that nanometre-scale magnetic structure information can be obtained even by using non-magnetic probe tips. Magnetization dependent measurements show that the canting of adjacent spins has no major influence on the electronic structure of the sample.

1. Introduction

As already proposed in the 1930s [1–3] magnetocrystalline anisotropy is mainly caused by the relativistic interaction between the electron spin and the electron's orbital angular momentum, better known as spin–orbit coupling (SOC). As a consequence the total energy of a magnetic sample depends on its magnetization direction. By convention the 'easy (hard) axis' is determined by the magnetization direction at which the total energy is minimized (maximized). In the past the band structure of thin ferromagnetic films has been analysed theoretically by several groups in order to identify the electronic origin of the magnetic anisotropy [4–8]. It was found that the electronic structure of ferromagnetic transition metals depends on whether

[3] Author to whom any correspondence should be addressed.
[4] Present address: IBM Research Division, T J Watson Research Center, Yorktown Heights, NY 10598, USA.
[5] Present address: National Renewable Energy Laboratory, Golden, CO 80401-3393, USA.

the sample is magnetized along its easy or hard axis because of 3d-band degeneracies which are lifted by SOC for one magnetization direction but not for the other [8].

However, the dependence of the electronic structure on the magnetization direction has never been confirmed experimentally by, e.g., angular resolved photoelectron spectroscopy, mainly due to the incompatibility of the experimental setup with the strong external magnetic field which is necessary to force the magnetization of the entire sample into the hard directions. We have chosen a different approach: by combining the high spatial resolution of scanning tunnelling microscopy with spectroscopic techniques we are able to detect the electronic structure of the sample locally. Since the tunnelling current of a scanning tunnelling microscope (STM), $I(\hat{e}_M(\boldsymbol{r}_\parallel), \boldsymbol{r}_\parallel, U)$, depends on the electronic structure of the sample we immediately expect that I depends on the magnetization direction $\hat{e}_M(\boldsymbol{r}_\parallel)$ of the sample. According to the model of scanning tunnelling spectroscopy (STS) by Tersoff and Hamann [9] the differential conductivity,

$$G(\boldsymbol{r}_\parallel, U) = \frac{\mathrm{d}I}{\mathrm{d}U}\bigg|(\boldsymbol{r}_\parallel, U) \propto n(\boldsymbol{r}_\parallel, z, \epsilon = E_\mathrm{F} + eU), \tag{1}$$

is proportional to the local density of states (LDOS) n of the sample at the lateral, $\boldsymbol{r}_\parallel$, and vertical, z, position of the tip at the energy of the bias voltage U, measured from the Fermi energy E_F. In the case of a magnetic sample the wavefunction of the sample is described by a spinor which is diagonalized by a majority $\psi_\uparrow|\uparrow\rangle$ and a minority $\psi_\downarrow|\downarrow\rangle$ spinor if the spin coordinate axis is parallel to the magnetization axis $\hat{e}_M$ and the SOC is omitted. Including the SOC in first-order perturbation theory, the change in the wavefunction $\psi_{\boldsymbol{k}_\parallel\nu}$ of state $|\boldsymbol{k}_\parallel\nu\rangle$ is proportional to the expectation value $\langle H_\mathrm{SO}\rangle\langle\sigma, \boldsymbol{k}_\parallel\nu|\boldsymbol{ls}|\sigma'\boldsymbol{k}_\parallel\nu'\rangle$ of the spin–orbit Hamiltonian. The orbital part of the matrix element $\langle\boldsymbol{ls}\rangle$ depends on the magnetization direction and can mix now majority and minority states as well as orbitals of the same spin channel, but of representations which had been orthogonal without SOC. The different representations can contribute quite differently to the tunnelling current. For example a slowly dispersing d_{z^2} state has a large tunnelling cross section, while an in-plane xy state has a small one. Thus we can divide the LDOS into a term n_0 independent of and a term $\Delta n(\hat{e}_M)$ dependent on the magnetization direction: $n(\hat{e}_M) = n_0 + \Delta n(\hat{e}_M)$. For a system with uniaxial anisotropy $\Delta n(\hat{e}_M) \propto \sin^2\varphi$, where φ is the angle between the magnetization direction and the easy axis.

Due to the high spatial resolution of STM we can make use of the intrinsic magnetic domain and domain wall structure of a sample in the remanent state, which immediately supplies regions oriented along the easy and hard anisotropy axes, respectively. We have chosen the Fe double layer (DL) on W(110) as a model system since its structural, electronic and magnetic properties are well known from prior spatial averaging [10–14] and local probe measurements [15–24] as well as from theoretical investigations [25, 26]. For example, it was recently found [23, 24] that smooth 1.5–2 monolayer (ML) thick Fe films grown on a low miscut W(110) substrate exhibit a distinct perpendicular magnetic stripe domain phase with a lateral periodicity of about 45 nm. Indeed, we found experimentally that the differential conductivity of the Fe DL on W(110) changes by of the order of 6% depending on whether the magnetization is directed along an easy or hard axis. This observation is corroborated by means of first-principles calculations. From a detailed analysis of the electronic structure we deduce how the signature of the magnetization direction is imprinted via the spin–orbit interaction. Our analysis reveals that the SOC of otherwise orthogonal bands leads to the formation of a small hybridization gap. This mixing of minority d_{z^2} and minority d_{xy+xz} states enhances the vacuum LDOS for one direction of the magnetization.

As an important implication of this effect the magnetic nanostructure of surfaces can be investigated with a conventional non-magnetic tip. An alternative but experimentally very

demanding method to obtain magnetic contrast which to our knowledge has not yet been implemented has been proposed by Bruno *et al* [27, 28] who suggested a two-terminal tip design to measure the spin asymmetry in the tunnelling conductance due to the spin–orbit scattering in the tip. The use of a nonmagnetic tip has the advantages that

(i) there is definitely no magnetic interaction between tip and sample which can conflict with the original magnetic state of the sample and

(ii) the preparation of a magnetic tip is omitted.

2. Experimental setup and calculational details

The experiments were performed in a five-chamber ultra-high vacuum (UHV) system with separate chambers for sample and tip distribution, substrate preparation, thin film deposition, conventional surface analysis (low energy electron diffraction, Auger electron spectroscopy etc) and low temperature STM using a home built instrument [29]. During the STM measurements the tip and the sample are held at a temperature $T = 14 \pm 1$ K. A superconducting magnet supplied a magnetic field normal to the surface plane. Tips were prepared by electrochemically etching a polycrystalline W wire. Upon introduction of the tip into the UHV system via a load lock the tip is briefly heated at a temperature $T \geqslant 2200$ K to remove tungsten oxides. For spin-sensitive experiments the tips were coated by a thin film of ferromagnetic material. The substrate is cleaned by cycles of oxidation at $T = 1500$ K and subsequent high temperature flashing ($T \geqslant 2200$ K) [30]. Fe films are grown by thermal evaporation from an Fe wire at a pressure $p \leqslant 2 \times 10^{-10}$ mbar onto the substrate held at $T \approx 500$ K. All topographic STM data were recorded in the constant current mode. The tunnelling spectra presented here were acquired by *scanning* the sample and measuring one $\mathrm{d}I/\mathrm{d}U$ spectrum at every pixel. After switching off the feedback loop an ac component ($U_{\mathrm{mod}} \leqslant 10$ mV, $\nu \approx 2$ kHz) is added to the gap voltage U which is ramped linearly, and 150 values of the lock-in signal are acquired. At the end of the ramp the modulation is switched off and the feedback is reactivated. In contrast, maps of the differential conductivity $\mathrm{d}I/\mathrm{d}U$ at a particular voltage U are measured with an active feedback circuit.

To interpret the experiments we have performed first-principles calculations based on the density functional theory. Using our FLEUR code which is an implementation of the full-potential linearized augmented plane wave (FLAPW) method in the film geometry [31, 32] including the SOC second variational procedure we have calculated the electronic structure of 2 ML Fe/W(110) as a function of the magnetization direction. The films consisted of five layers of W and two layers of Fe on each side of the film. For the structural model we used the experimental W lattice constant ($a_0 = 3.167$ Å) and relaxed the Fe layers by force calculations applying the generalized gradient approximation (GGA) [33]. Electronic structure calculations including spin–orbit interactions were carried out using the local density approximation (LDA) in the parametrization of Moruzzi *et al* [34]. Recently, this model provided a detailed understanding of the unusual magnetic reorientation transition of this system as a function of the film thickness. The structural optimization to determine the equilibrium interlayer distances was carried out neglecting the spin–orbit interaction. 33 special $\boldsymbol{k}_{\parallel}$ points in the irreducible wedge of the two-dimensional Brillouin zone (I-2D-BZ) (one-quarter of the BZ) of the chemical unit cell were used. The spin–orbit dependent contribution to the tunnelling current was described with a much larger set of $\boldsymbol{k}_{\parallel}$ points (mentioned in the text individually) in the magnetic I-2D-BZ (one-half of the BZ).

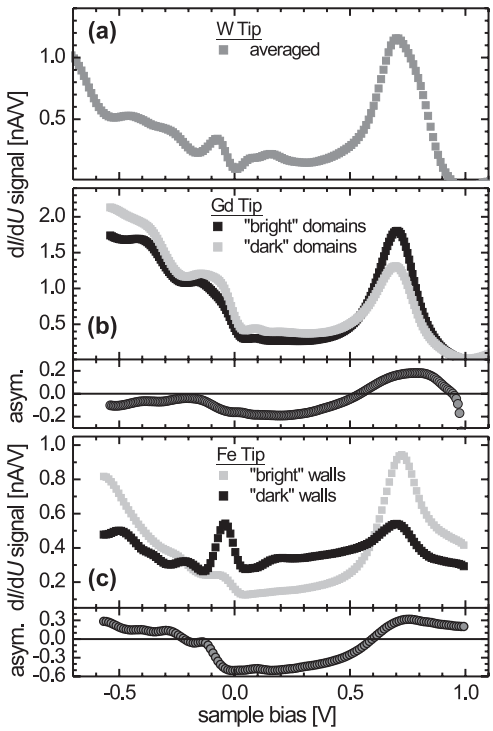

Figure 1. Averaged tunnelling $\mathrm{d}I/\mathrm{d}U$ spectra of the Fe DL on W(110) as measured with (a) a clean W tip, (b) an out-of-plane sensitive Gd coated tip and (c) an in-plane sensitive Fe coated tip. With magnetic tips a significant variation of the spectral intensity is found at different locations of the sample. These differences are responsible for the contrast in SP-STM images and are caused by SP tunnelling between the magnetic tip and the magnetic sample.

3. Results and discussion

The most widely used theory of STM has been developed by Tersoff and Hamann [9]. In the framework of this theory the STM is sensitive to the local density of electronic states (LDOS) which evanesce from a conducting surface out to the position of the atom at the tip apex. Constant current topographs simply represent the contour of a constant energy integrated LDOS. By means of spectroscopic techniques it is possible to get access to the differential conductivity $\mathrm{d}I/\mathrm{d}U$ which—at sufficiently low sample bias U—is proportional to the energy resolved LDOS [9]. Since conventional non-magnetic tip materials[6], e.g., W and PtIr, exhibit no spin polarization at the Fermi level both spin channels contribute equally to the total tunnelling current and the measured differential conductivity represents the spin averaged LDOS. As already mentioned above this paper will focus on 2 ML Fe/W(110), the so-called Fe DL, the structural, electronic and magnetic properties of which we know very well. Figure 1(a) shows an average of several hundred Fe DL spectra as measured with a clean W tip. The spectrum exhibits two main features: a relatively weak peak at a $U = -0.08$ V and a much stronger peak at $U = 0.7$ V. As will be discussed in more detail below comparison with theory reveals that these peaks are caused by two d_{z^2} states.

[6] In this context the term 'non-magnetic' denotes dia-or paramagnetic materials which, in contrast to ferromagnets, exhibit no spin polarization at the Fermi level.

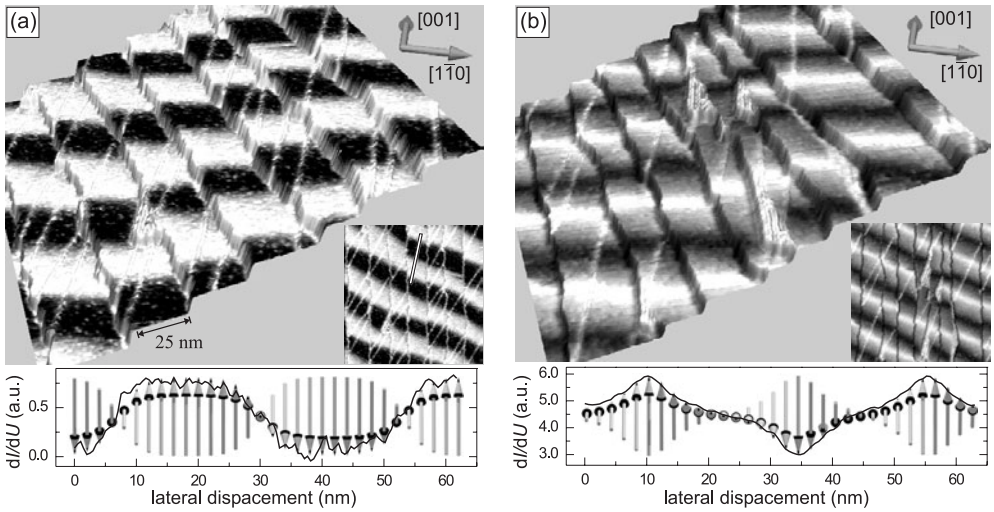

Figure 2. Rendered perspective representation of SP-STM data showing the topography (height) and the magnetic $\mathrm{d}I/\mathrm{d}U$ signal (grey scale) of 2.0 ± 0.05 ML Fe/W(110) as measured with different tips resulting in (a) out-of-plane and (b) in-plane contrast. Top view images of the $\mathrm{d}I/\mathrm{d}U$ signal are also presented as insets. Stripe domains with a perpendicular magnetization run along the [1$\bar{1}$0] direction. They are separated by domain walls of alternating magnetization direction. The line sections (bottom panel) reveal a periodicity of about 45 nm. The measurement parameters were (a) $I = 0.3$ nA, $U = -0.45$ V and (b) $I = 0.3$ nA, $U = +0.70$ V.

The experiment becomes spin sensitive if a magnetic tip material is used. Then, the differential conductivity can be written as [35]

$$\frac{\mathrm{d}I}{\mathrm{d}U}(\boldsymbol{r}_\parallel, U)_{\mathrm{SP}} = G(1 + P_{\mathrm{T}} P_{\mathrm{S}} \cos\varphi), \tag{2}$$

where $G = \mathrm{d}I/\mathrm{d}U(\boldsymbol{r}_\parallel, U)_{\mathrm{SA}}$ is the spin averaged differential conductance, $P_{\mathrm{T}} = P_{\mathrm{T}}(E_{\mathrm{F}})$ is the spin polarization of the tip at the Fermi energy and $P_{\mathrm{S}} = P_{\mathrm{S}}(E_{\mathrm{F}}+eU)$ is the spin polarization of the sample at the energy $E_{\mathrm{F}} + eU$. The spin polarizations of the tip and the sample are defined as $P_{\mathrm{S,T}}(E) \equiv (n^{\uparrow}_{\mathrm{S,T}}(E) - n^{\downarrow}_{\mathrm{S,T}}(E))/(n^{\uparrow}_{\mathrm{S,T}}(E) + n^{\downarrow}_{\mathrm{S,T}}(E))$ with $n^{\uparrow}_{\mathrm{S,T}}(E)$ and $n^{\downarrow}_{\mathrm{S,T}}(E)$ being the density of states of majority and minority electrons, respectively. The angle $\varphi = \varphi(\vec{M}_{\mathrm{T}}, \vec{M}_{\mathrm{S}}(\vec{r}))$ is enclosed by the tip magnetization $\vec{M}_{\mathrm{T}}$ and the local sample magnetization $\vec{M}_{\mathrm{S}}(\vec{r})$ below the tip apex. On an electronically homogeneous surface, $G(\boldsymbol{r}_\parallel)$ and P_{S} are independent of the location $\boldsymbol{r}_\parallel$. Therefore, any lateral variation of the $\mathrm{d}I/\mathrm{d}U$ signal is caused by the $\cos\varphi$ term, which—at a fixed tip magnetization direction—is directly connected to the local orientation of the sample magnetization $\vec{M}_{\mathrm{S}}(\boldsymbol{r}_\parallel)$. Figures 1(b) and (c) show $\mathrm{d}I/\mathrm{d}U$ spectra of the Fe DL on W(110) which have been measured with an out-of-plane sensitive Gd tip and an in-plane sensitive Fe tip, respectively, on different locations of the Fe DL which gave a high asymmetry in the spectra. Since the Fe DL on W(110) exhibits a perpendicular anisotropy a non-zero $\cos\varphi$ term in equation (2) must originate from domains if a Gd coated tip is used and from domain *walls* for an Fe coated tip. As indicated in equation (2) the strength of the measured asymmetry scales with the product of the spin polarization of tip *and* sample and therefore varies for different tips [19].

Figure 2 shows spin polarized (SP) STM data revealing the structural and magnetic properties of the Fe DL as epitaxially grown on a W(110) substrate with an average terrace width of 25 nm. After preparation the sample exhibits a macroscopically demagnetized state by periodically changing the magnetization direction between up and down. Figure 2(a),

which has been measured with a perpendicularly sensitive tip, shows that this is accomplished by the formation of stripe domains running along the $[1\bar{1}0]$ direction. As best visible in the line section of figure 2(a) (bottom panel) the measured magnetic periodicity amounts to about 45 nm. The orientation of the domain walls can be studied with an in-plane sensitive tip (figure 2(b)). Obviously, the magnetization direction alternates between opposite directions for adjacent domain walls. Since, however, we do not know the azimuthal orientation of the tip magnetization in our experimental setup we cannot determine experimentally whether the magnetization in the centre of the wall points in the [001] or in the $[1\bar{1}0]$ direction, i.e., whether the domain walls are Néel or Bloch walls. For domain walls in ultra-thin out-of-plane magnetized films it is energetically favourable to rotate the magnetization vector parallel to the wall plane (Bloch type) thereby avoiding magnetic charges. In this particular case a Bloch-type wall is also supported by the anisotropy of the Fe DL at higher temperature ($T \geqslant 160$ K) where the easy axis switches into the $[1\bar{1}0]$ direction, too [13]. The lower panel of figures 2(a) and (b) shows line profiles which have been measured across three domain walls. As indicated by the arrows the measured line profiles can be fitted by three winding 180° Bloch walls [21] using a standard wall profile $\sin(\varphi(x)) = \tanh((x - x_0)/(w/2))$ [36] with a wall width of $w = 7$ nm and a distance between wall centres of 23 nm.

Surprisingly, the magnetic structure of the sample can be imaged with a non-magnetic tip, too, which is not expected on the basis of equation (2). Figures 3(a) and (b) show the topography and the $\mathrm{d}I/\mathrm{d}U$ map at $U = +50$ mV of 1.75 ± 0.1 ML Fe/W(110). In other words, 75% of the W(110) substrate are covered with an Fe DL while 25% are covered with an ML of Fe. Since the ML exhibits a lower (spin averaged) differential conductivity (lower G in equation (2)) than the DL at this particular bias voltage, the former appears dark in figure 3(b). Two dislocation lines running along the [001] direction appear on the DL approximately in the centre of the image. While they are only weakly visible in the topography as 0.1–0.2 Å high elevations, intensive dark lines can be recognized in the $\mathrm{d}I/\mathrm{d}U$ map of figure 3(b), representing a change of the local electronic properties caused by local relaxation [17]. In the context of this article the most important feature is the periodically arranged dark lines in figure 3(b) which run along the $[1\bar{1}0]$ direction and which immediately remind us of the domain wall structure as imaged by means of SP-STS with an Fe coated tip (figure 2(b)). However, in contrast to the results of figure 2(b), the periodicity now amounts to 20–25 nm, i.e., half the periodicity measured with a magnetic tip, and all domain walls exhibit the same contrast. In order to get some insight into the origin of this contrast we have performed tunnelling spectroscopy in the sample bias range $-0.6\ \mathrm{V} \leqslant U \leqslant 1.0\ \mathrm{V}$. As revealed by the local tunnelling spectra (figure 3(c)) this contrast is caused by a tiny difference which is energetically located just above the Fermi level (see inset): while the $\mathrm{d}I/\mathrm{d}U$ spectrum measured with the tip positioned above the domain exhibits a weak peak at $U = 0.07$ V, this peak is almost absent in the domain wall spectra. This is further illustrated by the plot of the normalized difference

$$A(\boldsymbol{r}_\parallel, U) = \frac{G(\boldsymbol{r}_\parallel, U) - G(\bar{\boldsymbol{r}}_\parallel, U)}{G(\boldsymbol{r}_\parallel, U) + G(\bar{\boldsymbol{r}}_\parallel, U)}, \tag{3}$$

where $\boldsymbol{r}_\parallel$ ($\bar{\boldsymbol{r}}_\parallel$) is the position of a domain (domain wall). The result is plotted in the lower panel of figure 3(c). However, if the normalized difference is calculated on the original data (as measured), a pronounced oscillation can be found just below the Fermi level, i.e. at small negative sample bias. As we will understand later by comparison with theoretical data this oscillation is not caused by any additional or missing spectroscopic features in the domain wall $\mathrm{d}I/\mathrm{d}U$ spectrum with respect to the spectrum measured at domains but by an overall energetical shift $\Delta E = 11$ meV. The physical origin is different work functions in domains and domain walls as already proposed in [4–6]. It can be corrected by shifting the domain

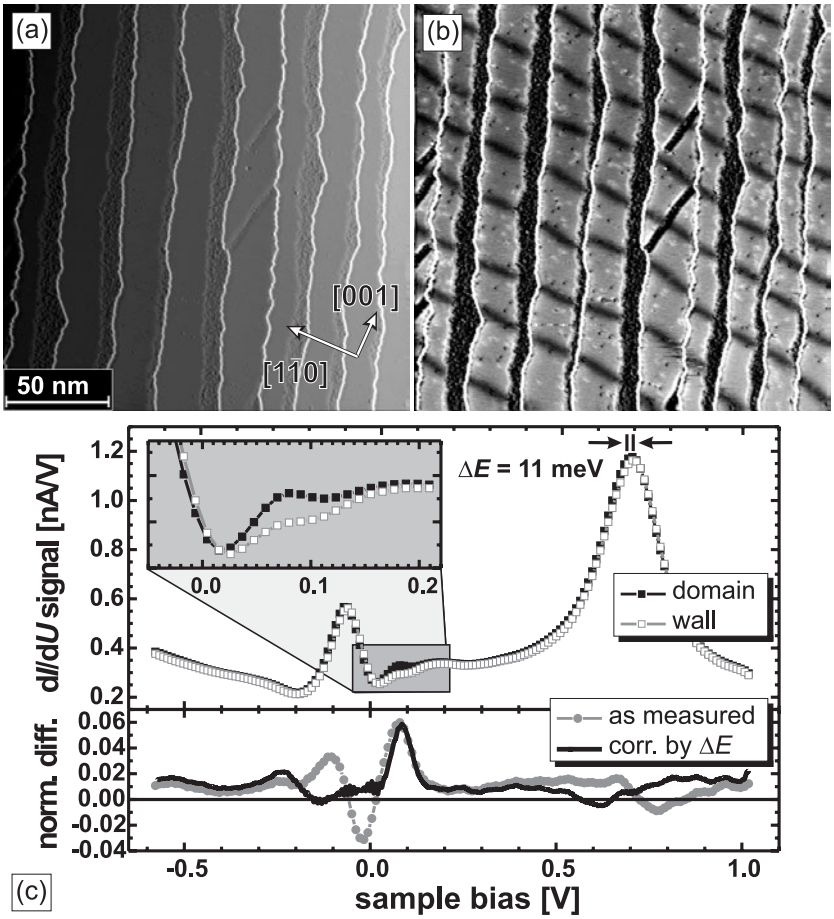

Figure 3. (a) Topography and (b) simultaneously measured $\mathrm{d}I/\mathrm{d}U$ map at $U = +50$ mV of 1.75 ± 0.1 ML Fe/W(110). Periodically arranged dark lines running along the [1$\bar{1}$0] direction are visible. The measured periodicity is half the magnetic periodicity as determined in figure 2 indicating that the contrast is caused by different (spin averaged) electronic properties of domains and domain walls. (c) Comparison of tunnelling spectra measured above domains and domain walls reveals that the contrast in (b) is caused by a small peak at $U = +70$ mV which is absent above the domain walls. The domain wall spectrum is shifted by + 11 mV with respect to the domain spectrum. The voltage bias dependent normalized difference between both spectra is plotted in the lower panel. A strong oscillation occurs around the Fermi level.

wall spectrum by $-\Delta E$. After this procedure the oscillation below E_{F} has almost perfectly disappeared.

In order to understand the reason for the changes in the ST spectra we have performed first-principles calculations of the electronic structure of 2ML Fe/W(110). From the model of Tersoff and Hamann we know that the vacuum LDOS should compare directly to the measured differential conductivity as stated before. Figure 4 shows the calculated vacuum LDOS, $n(E)$, at a tip–sample distance of about 14 Å for two different magnetization directions of Fe: out of plane, representing the magnetization state (full curve) in the domain, and in plane along the [1$\bar{1}$0] direction (dashed curve) as a model of the magnetization in the domain wall. There is a nice agreement of this plot with the experimental data of figure 3. We find two d_{z^2} states

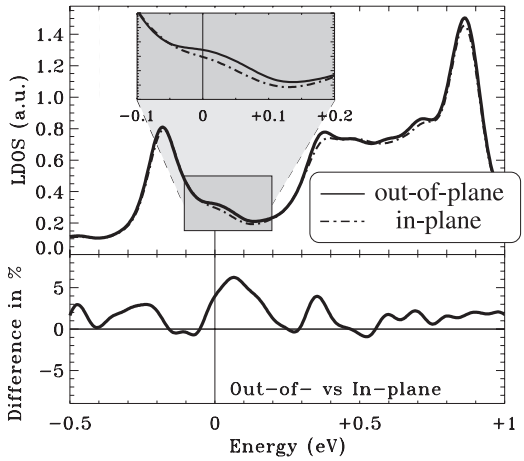

Figure 4. Calculated LDOS at about $z = 14$ Å above the surface of the Fe DL on W(110). The solid (dashed) curve in the upper panel shows the LDOS with the magnetization perpendicular to the film surface (in the film surface along the $[1\bar{1}0]$ direction). The lower panel displays the normalized difference. For the calculation 3600 $\boldsymbol{k}_\parallel$ points have been used in a square centred at $\overline{\Gamma}$ with an area covering 25% of the BZ (see figure 6).

from the Fe DL leading to pronounced peaks at −0.18 and +0.85 eV. These states are located at the $\overline{\Gamma}$ point of the 2D-BZ and therefore they are easily detectable by STS [37]. In fact, they can be identified with the peaks at −0.08 and +0.7 V which have been found in the experimental spectra shown in figure 1(a). The distinct shoulder at +0.35 eV in the calculated vacuum LDOS falls off much more rapidly with increasing distance from the surface than the d_{z^2} states which is probably the reason why it is absent in the experimental data. A spin analysis reveals that the peaks are caused by electronic states of minority character (neglecting the small spin mixing due to the spin–orbit interaction). A closer look (cf inset in figure 4) reveals a significant enhancement of the LDOS for the out-of-plane magnetized film within the energy range $-50\ \text{meV} \leqslant E \leqslant +150$ meV. The lower panel of figure 4 shows the normalized difference. Three peaks centred at about −300, +60 and +350 meV can be recognized. The most pronounced peak at +60 meV in the normalized difference is in very nice agreement with the experimental observation (cf figure 3(c)). Even the smaller peak at −300 meV is in accordance with the experimental findings. The peak at +350 meV, on the other hand, is related to the calculated LDOS shoulder and thus absent in the experimental data.

One can find the origin of the changes in the LDOS by analysing the different contributions in $\boldsymbol{k}_\parallel$ space for the two directions of the film magnetization. The upper panels of figure 5 show plots of the $\boldsymbol{k}_\parallel$-resolved contributions over the 2D-BZ of the minority projected part of the LDOS for the out-of-plane direction while the lower panels display the difference between out-of-plane and in-plane magnetization directions. Five different energies in the interval $-50\ \text{meV} \leqslant E \leqslant +150$ meV have been selected[7]. For the LDOS at large distances from the surface only states in the vicinity of the $\overline{\Gamma}$ point give a considerable contribution. Thus we can concentrate on a small circle around the $\overline{\Gamma}$ point. We can see that with increasing energy of the plots a bright spot at the $\overline{\Gamma}$ point indicating a large LDOS contribution first appears and then disappears again. The other major contribution to the LDOS is related to two stretched spots

[7] All states have been smeared by a Gaussian function with half width at half maximum of 50 meV. This broadening does not reflect thermal effects—as we described above the spectroscopic measurements have been performed at low temperature ($T = 14 \pm 1$ K)—but smoothens the results to compensate for the use of a finite $\boldsymbol{k}_\parallel$ mesh.

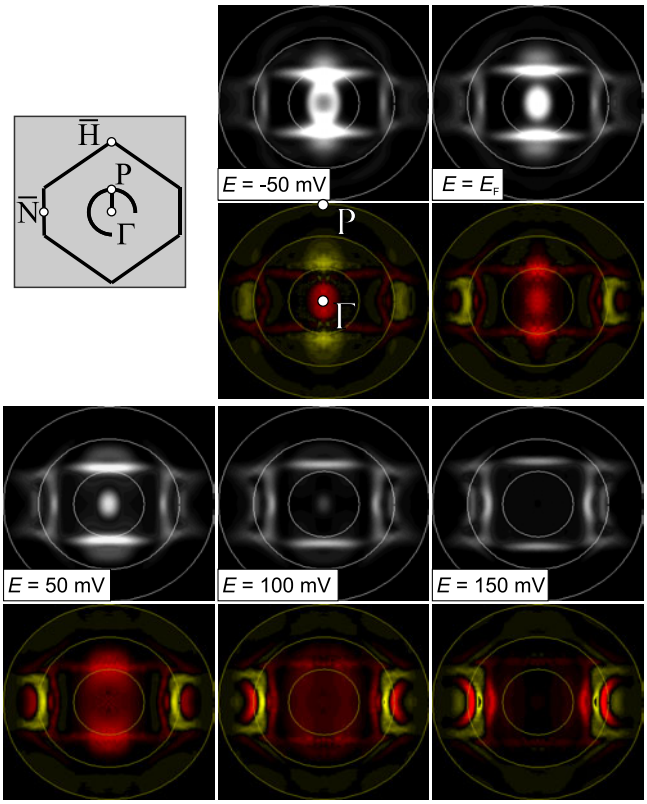

Figure 5. Calculated LDOS above the perpendicularly magnetized Fe DL on W(110) (top panel) and difference between the LDOS for out-of-plane and in-plane magnetization directions (bottom panel) plotted for five different energies -50 meV $\leqslant E \leqslant +150$ meV. As can be recognized in the top left view of the surface Brillouin zone the point 'P' lies at about 1/3 $\overline{\Gamma\mathrm{H}}$. Red (yellow) represents an enhancement (reduction) of the density of states. 6000 $\boldsymbol{k}_{\parallel}$ points have been used to sample the disc.

(This figure is in colour only in the electronic version)

at the inner circle in the $\overline{\Gamma\mathrm{P}}$ direction. They shift a little outwards with increasing energy. As we will show below in figure 6 this is due to the dispersion of the responsible band. If we now focus on the difference plots, i.e. the lower panels of figure 5, we observe that at the Fermi energy $E = E_{\mathrm{F}}$ and 50 meV above it the higher (2D BZ integrated) out-of-plane LDOS can be related to (red) spots at the inner circle in the $\overline{\Gamma\mathrm{P}}$ direction[8]. At the other energies there is only a negligible 2D BZ integrated difference between the two magnetization directions as we have also concluded from figure 4.

With the additional information from the $\boldsymbol{k}_{\parallel}$ space resolved LDOS that the origin of the LDOS change comes from an effect in the $\overline{\Gamma\mathrm{P}}$ direction we can clarify the electronic origin from a band structure plot along that direction presented in figure 6. A vertical line in the plots indicates the position of the inner circle of figure 5 for comparison. In figure 6(a) the spin–orbit interaction is turned off, and majority and minority states diagonalize the Hamiltonian. We find that in the $\boldsymbol{k}_{\parallel}$ region of interest, i.e. at the inner circle, three minority state bands cross

[8] The differences at the centre circle in the direction perpendicular to $\overline{\Gamma\mathrm{P}}$ are due to bands shifted a little in $\boldsymbol{k}_{\parallel}$ space. Thus the positive and negative contributions compensate after integration over the 2D-BZ.

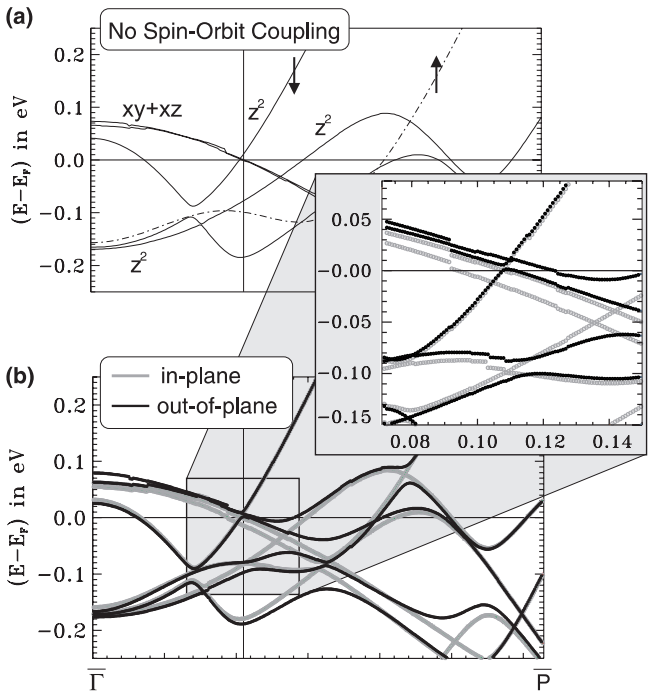

Figure 6. Comparison of the band structure of the Fe DL on W(110) along the line $\overline{\Gamma\mathrm{P}}$ (cf figure 5) (a) without and (b) with spin–orbit interaction. In (a) the full (dot–dashed) curve represents the minority (majority) bands. The region of interest is shown at higher resolution in the inset. The vertical lines at about 1/3 $\overline{\Gamma\mathrm{P}}$ indicate the radius of the inner circle of figure 5. 400 $\boldsymbol{k}_{\parallel}$ points along $\overline{\Gamma\mathrm{P}}$ have been used to plot the band structure.

at the Fermi energy. One is rising while two nearly degenerate ones are falling. While the rising band is of d_{z^2} character, the two others consist of states which are linear combinations of d_{xy} and d_{xz} orbitals. Note that states with d_{xy} and d_{xz} orbital character contribute only by a negligible amount to the vacuum LDOS, and d_{z^2} states often dominate the vacuum LDOS. Since the d_{z^2} band in figure 6(a) (without SOC) is rather steep it contributes only little to the LDOS above the sample surface. However, depending on the magnetization direction the SOC can mix the three crossing bands. As one can see in the inset of figure 6(b) the mixing occurs in the case of out-of-plane magnetization direction leading to a hybridization gap between one of the d_{xy+xz} bands and the d_{z^2} band. The introduction of this gap changes the dispersion of the d_{z^2} state (making it even flat at the hybridization gap) upon changing the magnetization direction which explains the detected enhancement of the LDOS in the STS.

Figures 7(a) and (b) show the topography and the $\mathrm{d}I/\mathrm{d}U$ map at $U = +50$ mV of 1.8 ± 0.1 ML Fe/W(110), respectively. It becomes apparent from the line section (figure 7(c)) which has been drawn along the line in figure 7(b) that the wall profile is significantly narrower than in the SP measurements (figure 2(c)). This finding is easily comprehensible if we bring to mind that the magnetocrystalline energy density and therefore $\Delta n(\hat{e}_M)$, which both have their origin in the SOC, of a uniaxial magnetic material scale with $\sin\varphi^2$, while—according to equation (2)—the projection of the magnetization as measured with a magnetic tip scales with $\sin\varphi$, where φ is the angle between the magnetization $\vec{M}_{\mathrm{S}}(\vec{r})$ and the film normal. We have tried to fit the domain wall profile of the wall which is marked by an arrow in figure 7(c)

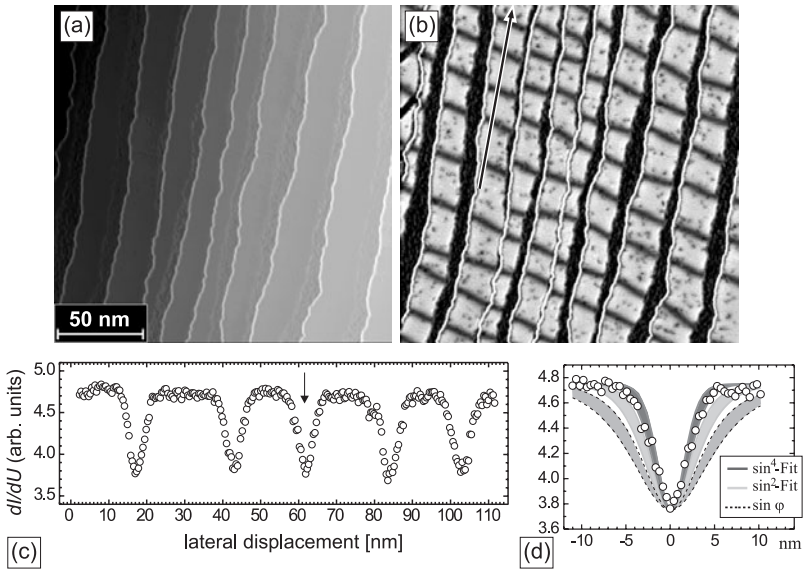

Figure 7. (a) Topography and (b) $\mathrm{d}I/\mathrm{d}U$ map at $U = +50$ mV of 1.8 ± 0.1 ML Fe/W(110). (c) Line section of the $\mathrm{d}I/\mathrm{d}U$ signal drawn across five domain walls along the line in (b). (d) The domain wall marked by an arrow in (c) has been fitted with $(\sin\varphi)^n$, $n = 1$, 2 and 4. We have assumed a domain wall width $w = 7 \pm 1$ nm. A reasonable agreement is achieved for $n = 2$ and 4.

and which is plotted on an expanded lateral scale in figures 7(d) by the function

$$y(x) = y_0 + y_{\mathrm{sp}} \left| \sin \left\{ \arcsin \left[\tanh \left(\frac{x - x_0}{w/2} \right) \right] + \pi/2 \right\} \right|^n , \tag{4}$$

where $y(x)$ is the $\mathrm{d}I/\mathrm{d}U$ signal measured at position x, x_0 is the position of the domain wall, w is the wall width and y_0 and y_{sp} are the spin averaged and SP $\mathrm{d}I/\mathrm{d}U$ signal. For $n = 1$ the fit function reduces to the standard domain wall profile as measured with a magnetic tip [24] and described by continuum micromagnetic theory [36]. Obviously, using a domain wall width $w = 7 \pm 1$ nm the data cannot be fitted satisfactorily for $n = 1$: as expected the resulting theoretical profile is much wider than the experimental data. Surprisingly, even for $n = 2$ the fit is still slightly wider than the measured profile. Therefore, we have also included a fit for $n = 4$. Now, the fit is slightly narrower than the measured profile which may be caused by a non-vanishing lateral decay length of the involved electronic states. We have to conclude this part by the statement that on the basis of the experimental data available we are currently not able to determine the exponent n precisely. It may have any value between $n = 2$ and 4. We have, however, performed further calculations in order to control how sensitive the spin–orbit induced effects on the electronic structure are to the tilt angle of the magnetization with respect to the out-of-plane direction. We have taken three intermediate steps: $\varphi = 22.5°$, 45° and 67.5°. While the reduction in the LDOS above the Fermi energy is below the limits of uncertainty for $\varphi = 22.5°$, it was significant for $\varphi = 45°$ and 67.5° which explains—compared to the result obtained with an Fe coated tip—the apparently reduced domain wall width as measured with the W tip (cf figures 2(b) and 3(b)). We have also calculated the electronic structure of the Fe DL on W(110) when the magnetization is oriented in plane along the [001] direction. The result is not consistent with the experimental result of figure 3(c) thereby confirming the above statement that the domain walls in the Fe DL are Bloch walls.

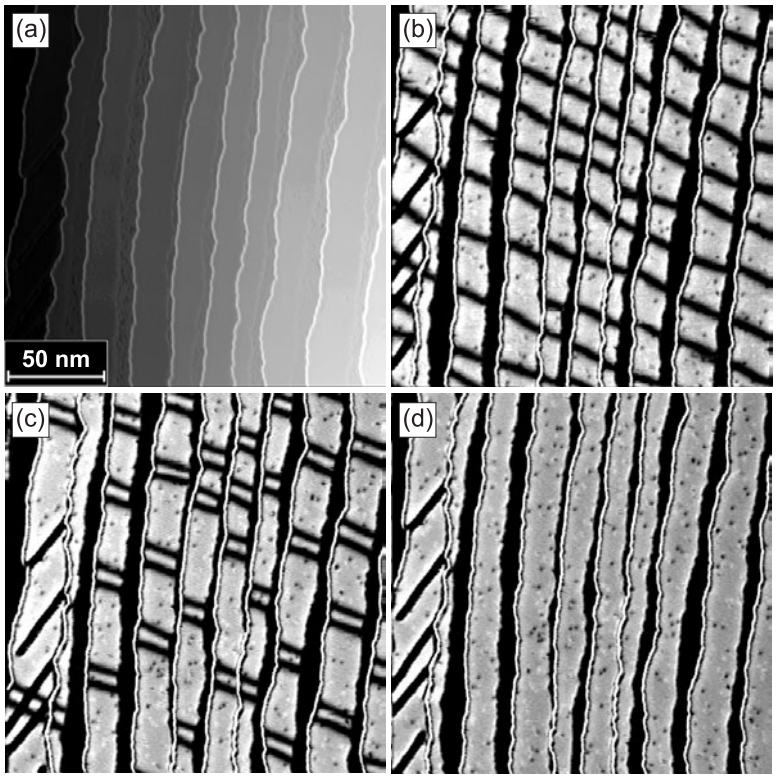

Figure 8. (a) Topography and dI/dU map at $U = +50$ mV of 1.7 ± 0.1 ML Fe/W(110) at (b) $\mu_0 H_{ext} = 0$ mT, (c) 600 mT and (d) 1000 mT. At $\mu_0 H_{ext} = 600$ mT the domains oriented parallel to the external field have expanded at the expense of the antiparallel domains leading to a continuous spin rotation. A field of 1000 mT is sufficient to saturate the sample completely.

There is another interpretation of the effect found experimentally which has not yet been discussed: beside spin–orbit effects the electronic properties might as well be changed by the canting of adjacent (atomic) spins which certainly exists within the domain wall where the magnetization rotates gradually. In order to exclude this possibility we have performed measurements at increasing external magnetic fields. Figure 8 shows the topography and maps of the dI/dU signal at $U = +50$ mV of 1.7 ± 0.1 ML Fe/W(110). Again, a periodic pattern of almost parallel dark lines along the $[1\bar{1}0]$ direction can be recognized in the Fe DL at zero field. As discussed above the lines represent domain walls of alternating in-plane magnetization (see figure 2(b)). Between the domain walls the Fe DL is perpendicularly magnetized. The orientation of these domains also alternates thereby forming a magnetization spiral along a particular DL nanowire [23]. Upon application of a perpendicular external field the domain oriented parallel with respect to the field grows at the expense of the domain oriented antiparallel. This implies a movement of the domain walls: the pairs of domain walls confining a domain antiparallel to the external magnetic field merge while the pairs confining a parallel domain move away from each other. At $\mu_0 H_{ext} = 600$ mT (figure 8(c)) the antiparallel domain is so strongly compressed between the surrounding walls that the magnetization basically performs a continuous 360° wall rotation [21]. If the canting of adjacent spins were responsible for the observed decrease of the dI/dU signal at $U = +50$ mV the whole 360° wall should appear dark in figure 8(c). This is in contrast to the data which show two distinct domain walls

about 7 nm apart from each other. Consequently, we can exclude that the canting of adjacent spins causes the domain wall contrast when using non-magnetic tips.

4. Summary and outlook

In summary, we have shown by STS that the local electronic structure of 2 ML Fe/W(110) depends on whether the magnetization points along a hard or easy axis. *Ab initio* calculations reveal that the observed difference is caused by SOC which leads to the mixing between minority d_{xy+xz} and minority d_{z^2} spin states, the latter of which giving a higher contribution to the tunnelling current. This allows an imaging of magnetic nanostructures by means of conventional, i.e., non-spin-polarized STS. The effect has been observed on 2 ML Fe/W(110) using many different tip materials, namely W, Mn, Cr, Fe and Gd tips. Since the magnetization dependent term of the LDOS $\Delta n(\hat{e}_M) \propto \sin^2 \varphi$ it is believed that the effect is even visible on samples with rather broad domain walls. Furthermore, our theoretical results indicate that similar effects can also be found on Fe films on Mo(110), a system which exhibits a much smaller SOC. Therefore, we expect that the effect should be quite general and applicable to a large variety of systems.

Acknowledgments

Financial support from the Deutsche Forschungsgemeinschaft (grant Wi1277/16–1 and Graduiertenkolleg 'Physik Nanostrukturierter Festkörper') is gratefully acknowledged.

References

[1] Bloch F 1930 *Z. Phys.* **61** 206
[2] Bloch F and Gentile G 1931 *Z. Phys.* **63** 395
[3] van Vleck J H 1937 *Phys. Rev.* **52** 1178
[4] Slonczewski J C 1962 *J. Phys. Soc. Japan Suppl.* B1 **17** 34
[5] Darby M I and Isaac E D 1974 *IEEE Trans. Magn.* **10** 259
[6] Daalderop G H O, Kelly P J and Schuurmans M F H 1994 *Phys. Rev.* B **50** 9989
[7] Wu R and Freeman A J 1999 *J. Magn. Magn. Mater.* **200** 498
[8] Lessard A, Moos T H and Hübner W 1997 *Phys. Rev.* B **56** 2594
[9] Tersoff J and Hamann D R 1985 *Phys. Rev.* B **31** 805
[10] Elmers H J and Gradmann U 1990 *Appl. Phys.* A **51** 255
[11] Elmers H J, Hauschild J, Fritzsche H, Liu G, Gradmann U and Köhler U 1995 *Phys. Rev. Lett.* **75** 2031
[12] Sander D, Skomski R, Schmidthals C, Enders A and Kirschner J 1996 *Phys. Rev. Lett.* **77** 2566
[13] Hauschild J, Gradmann U and Elmers H J 1998 *Appl. Phys. Lett.* **72** 3211
[14] Elmers H J, Hauschild J and Gradmann U 1999 *Phys. Rev.* B **59** 3688
[15] Bethge H, Heuer D, Jensen C, Reshöft K and Köhler U 1995 *Surf. Sci.* **331–333** 878
[16] Jensen C, Reshöft K and Köhler U 1996 *Appl. Phys.* A **62** 217
[17] Bode M, Pascal R, Dreyer M and Wiesendanger R 1996 *Phys. Rev.* B **54** 8385
[18] Pietzsch O, Kubetzka A, Bode M and Wiesendanger R 2000 *Phys. Rev. Lett.* **84** 5212
[19] Bode M, Pietzsch O, Kubetzka A and Wiesendanger R 2001 *J. Electron Spectrosc. Relat. Phenom.* **114–116** 1055
[20] Bode M, Pietzsch O, Kubetzka A, Heinze S and Wiesendanger R 2001 *Phys. Rev. Lett.* **86** 2142
[21] Pietzsch O, Kubetzka A, Bode M and Wiesendanger R 2001 *Science* **292** 2053
[22] Kubetzka A, Pietzsch O, Bode M and Wiesendanger R 2001 *Phys. Rev.* B **63** 140407
[23] Bode M, Kubetzka A, Pietzsch O and Wiesendanger R 2001 *Appl. Phys.* A **72** S149
[24] Kubetzka A, Bode M, Pietzsch O and Wiesendanger R 2002 *Phys. Rev. Lett.* **88** 057201
[25] Hong S C, Freeman A J and Fu C L 1988 *Phys. Rev.* B **38** 12156
[26] Elmers H J 1998 *J. Magn. Magn. Mater.* **185** 274
[27] Bruno P 1997 *Phys. Rev. Lett.* **79** 4593

[28] Pareek T P and Bruno P 2001 *Phys. Rev.* B **63** 165424
[29] Pietzsch O, Kubetzka A, Haude D, Bode M and Wiesendanger R 2000 *Rev. Sci. Instrum.* **71** 424
[30] Bode M, Pascal R and Wiesendanger R 1995 *Surf. Sci.* **344** 185
[31] Wimmer E, Krakauer H, Weinert M and Freeman A J 1981 *Phys. Rev.* B **24** 864
[32] Weinert M, Wimmer E and Freeman A J 1982 *Phys. Rev.* B **26** 4571
[33] Perdew J P, Chevary J A, Vosko S H, Jackson K A, Pederson M R, Singh D J and Fiolhais C 1992 *Phys. Rev.* B **46** 6671
[34] Moruzzi V L, Janak J F and Williams A R 1978 *Calculated Electronic Properties of Metals* (New York: Pergamon)
[35] Wortmann D, Heinze S, Kurz P, Bihlmayer G and Blügel S 2001 *Phys. Rev. Lett.* **86** 4132
[36] Hubert A and Schäfer R 1998 *Magnetic Domains* (Berlin: Springer)
[37] Stroscio J A, Pierce D T, Davies A, Celotta R J and Weinert M 1995 *Phys. Rev. Lett.* **75** 2960